EMBOJ-2016-96012

Malyutin et al

Appendix

Table of Contents

Figure S1. Time course of GTP hydrolysis.

Figure S2. Cryo-EM map of 60S-Nmd3 with FSC curves and Resmap figures.

Figure S3. 60S-Nmd3 processing scheme.

Figure S4. 60S-Nmd3-Lsg1 processing scheme.

Figure S5. 60S-Nmd3-Lsg1-Tif6 (60SNLT) dataset collected on Titan Krios.

Figure S6. 60S-Nmd3-Lsg1-Tif6 (60SNLT) set 2 processing scheme.

Figure S7. Processing schematic for the combined dataset used to refine a 3.1A map with focus on 60S-Nmd3 density.

Figure S8. Re-processing scheme for 60S-Nmd3-Lsg1-Tif6 dataset collected on Titan Krios using native pixel size of 1.09 Å/pix, MotionCor2 for frame alignment and Relion2-Beta for processing.

Figure S9. Nmd3 binding site determined by cryo-EM versus UV crosslinking.

Figure S10. eL41 does not affect Lsg1 function.

Figure S11. Overlay of Lsg1 and YlqF

Figure S12. Depletion of Lsg1 traps Nmd3 but not Tif6 in the cytoplasm.

Supplemental Tables

Table S1. Descriptions of various states of L1 stalk, Nmd3, and Lsg1 isolated during processing of the datasets.

Table S2. Predicted hydrogen bonds and salt bridges among Nmd3, eL42 and uL1 and comparison with those of eIF5A (PDBePISA server)

Table S3. Strains used in this study

Table S4. Plasmids used in this study

Table S5. Summary of data collected, particles extracted, number of particles used for classification and refinement

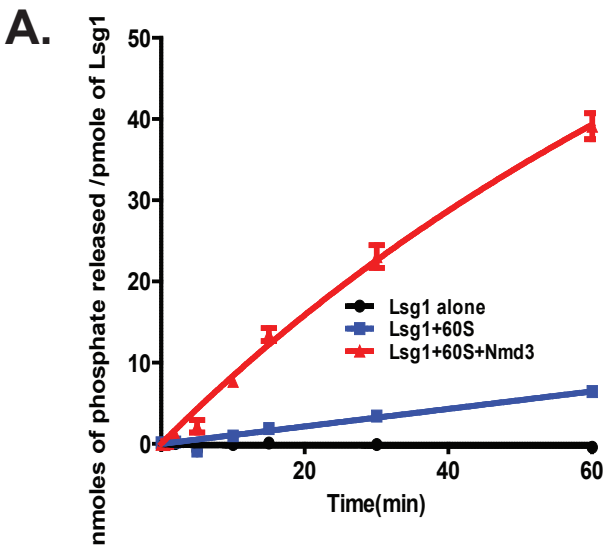

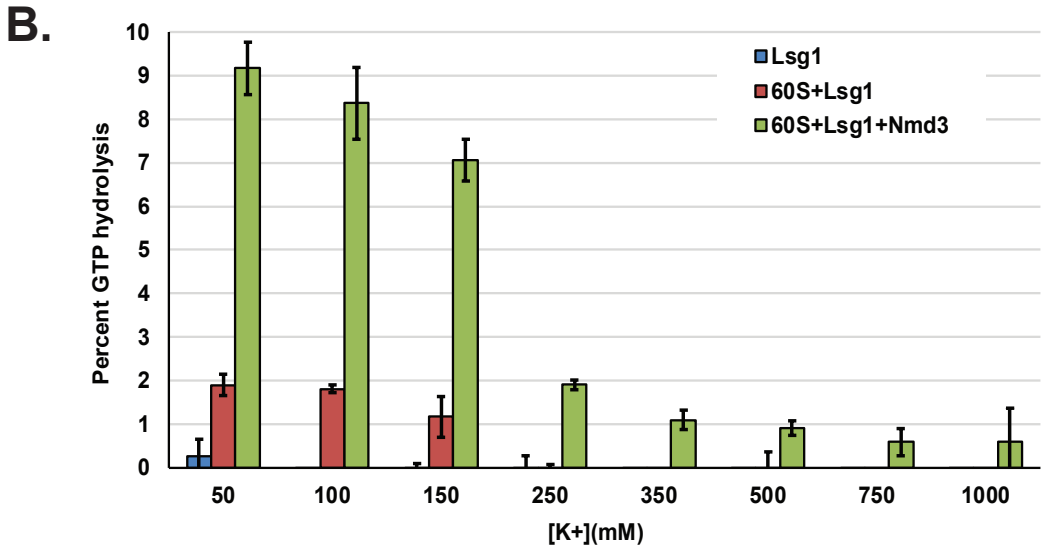

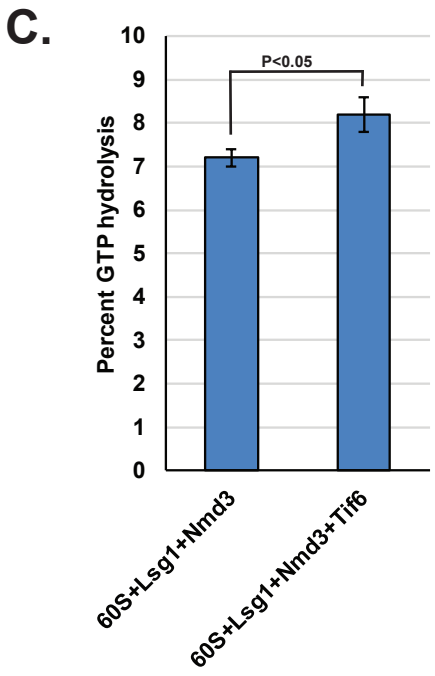

Figure S1. Characterization of Lsg1 GTPase activity. (A) Time course of GTP hydrolysis. GTPase activity of Lsg1 was measured as phosphate released over time in reactions containing 125nM Lsg1 alone, 125nM Lsg1 plus 25nM 60S subunit, and 125nM Lsg1 plus 25nM 60S subunit and 100nM Nmd3. (B) Free Lsg1 is not activated by elevated levels of K+ ions while 60S or 60S and Nmd3 stimulated activation of Lsg1 is inhibited. Percent GTP hydrolysis by 250nM free Lsg1 or in combination with 25nM 60S or 25nM 60S+100nM Nmd3 was measured at [K+] ranging from 50mM to 1M. (C) Lsg1 shows stimulation of GTPase activity in response to addition of Tif6. Percent GTP hydrolysis by 250nM Lsg1 was measured in presence of 25nM 60S and 100nM Nmd3 and with or without 125nM Tif6. All experiments were done in triplicate and mean and standard deviation are shown. A two-tailed T-test was used for calculating P value in (C).

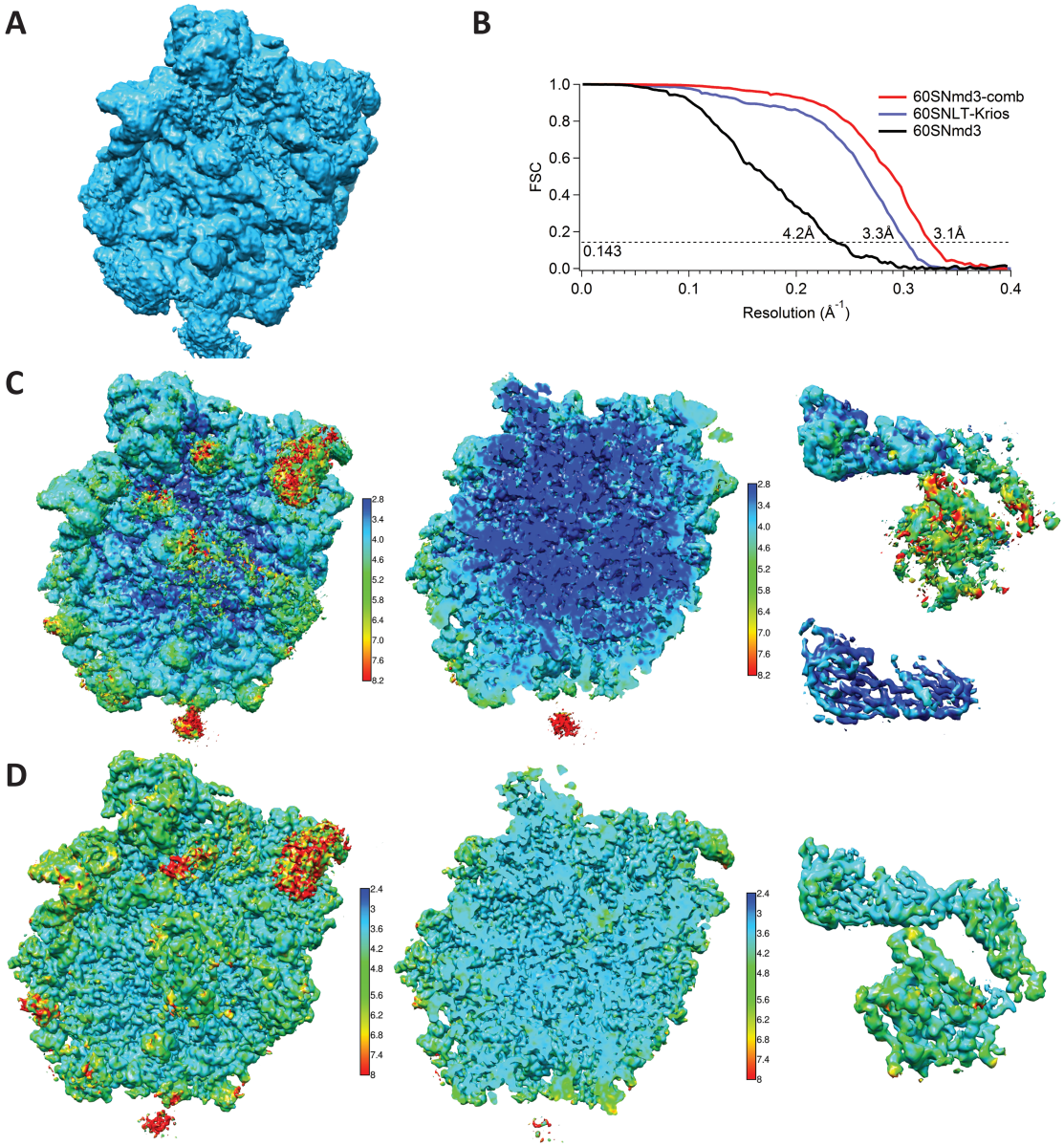

Figure S2. Cryo-EM map of 60S-Nmd3 with FSC curves and Resmap figures. (A) Map of 60S-Nmd3 only complex. (B) FSC curves for the 60S-Nmd3 (black), 60S-Nmd3-Lsg1-Tif6-GMPPNP (blue), and 60S-Nmd3 combined dataset (red). (C) 60S-Nmd3 combined map colored by resolution. Magnified segmented Nmd3 and Lsg1 densities are shown on the right at two thresholds. (D) 60SNLT map colored by resolution. Magnified segmented Nmd3 and Lsg1 densities are shown on the right.

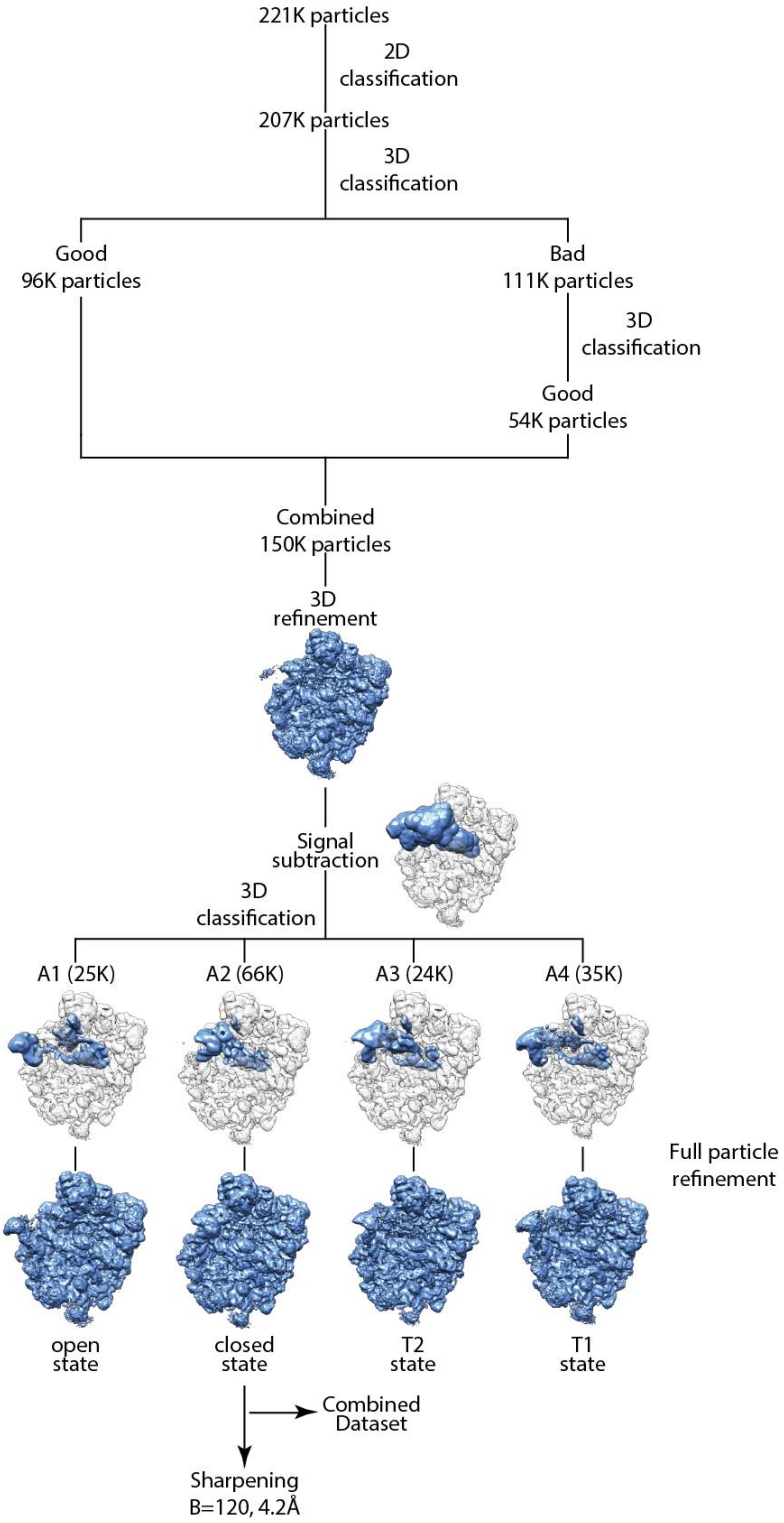

Figure S3. 60S-Nmd3 processing scheme. After the 1st round of 3D classification, the "bad" particles were classified again and the two sets of good particles were merged for further processing. The density maintained during signal subtraction is shown in blue. Good 3D classes and number of particles contributing to those classes are shown. Refined classes are described in Table S4. Particles from class2 after signal subtraction and 3D classification were used in a combined dataset to focus on Nmd3 density.

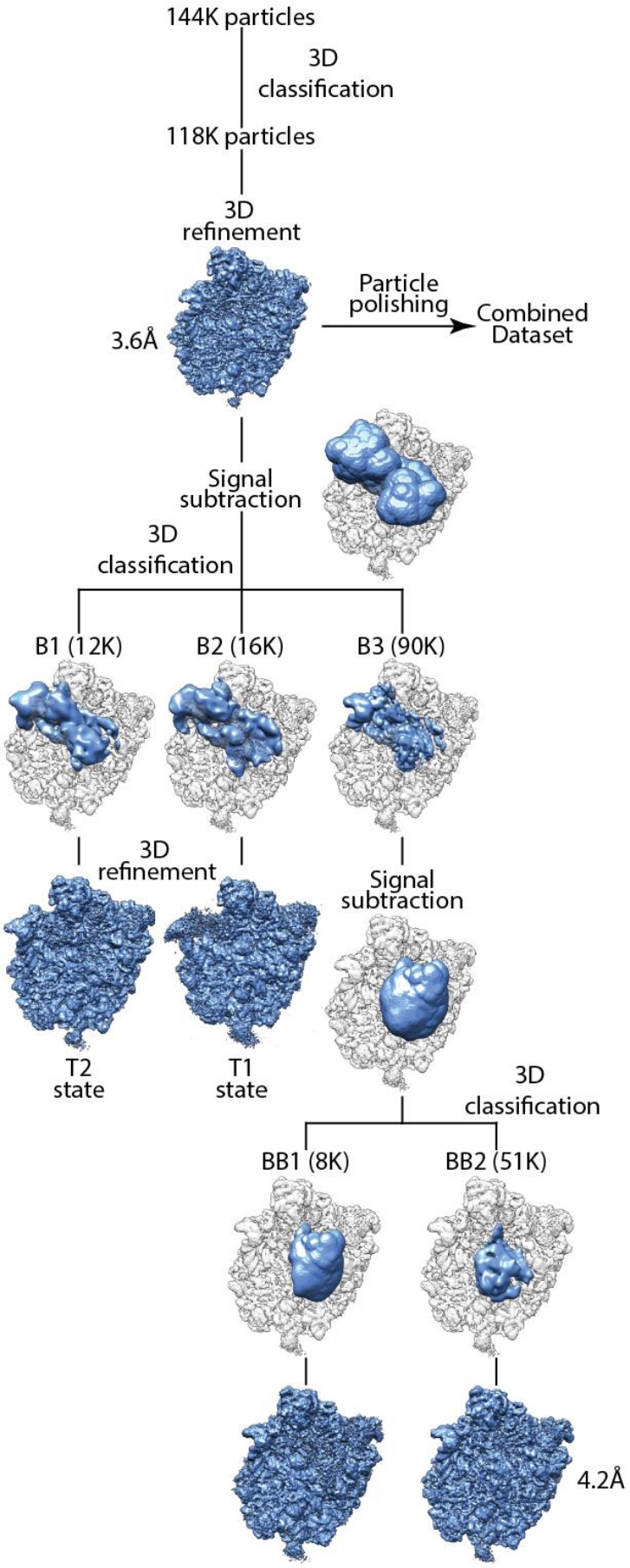

Figure S4. 60S-Nmd3-Lsg1 processing scheme. The density maintained during signal subtraction is shown in blue. Particles after the first round of 3D classification were polished and used in a combined dataset to focus on Nmd3 density. Further rounds of signal subtraction and 3D classification were performed to capture various states of L1 stalk, Nmd3, and Lsg1. Refined classes are described in Table S4.

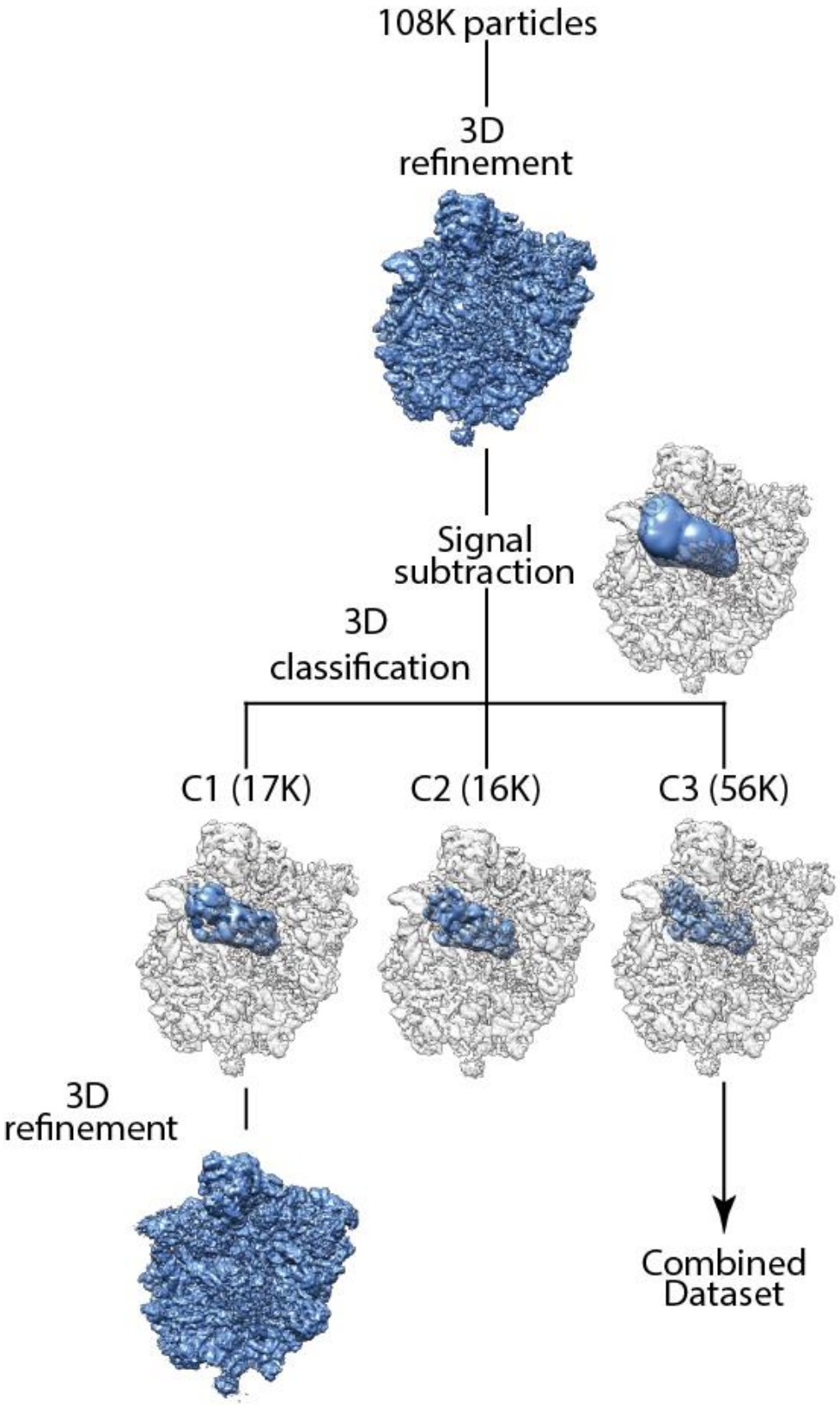

Figure S5. 60S-Nmd3-Lsg1-Tif6 (60SNLT) dataset collected on Titan Krios. The particles were binned from the original pixel size of 1.1Å/pix to 1.26 Å/pix in order to match the other data sets acquired on FEI Tecnai F-30. The density maintained during signal subtraction is shown in blue. Refined classes are described in Table S4.

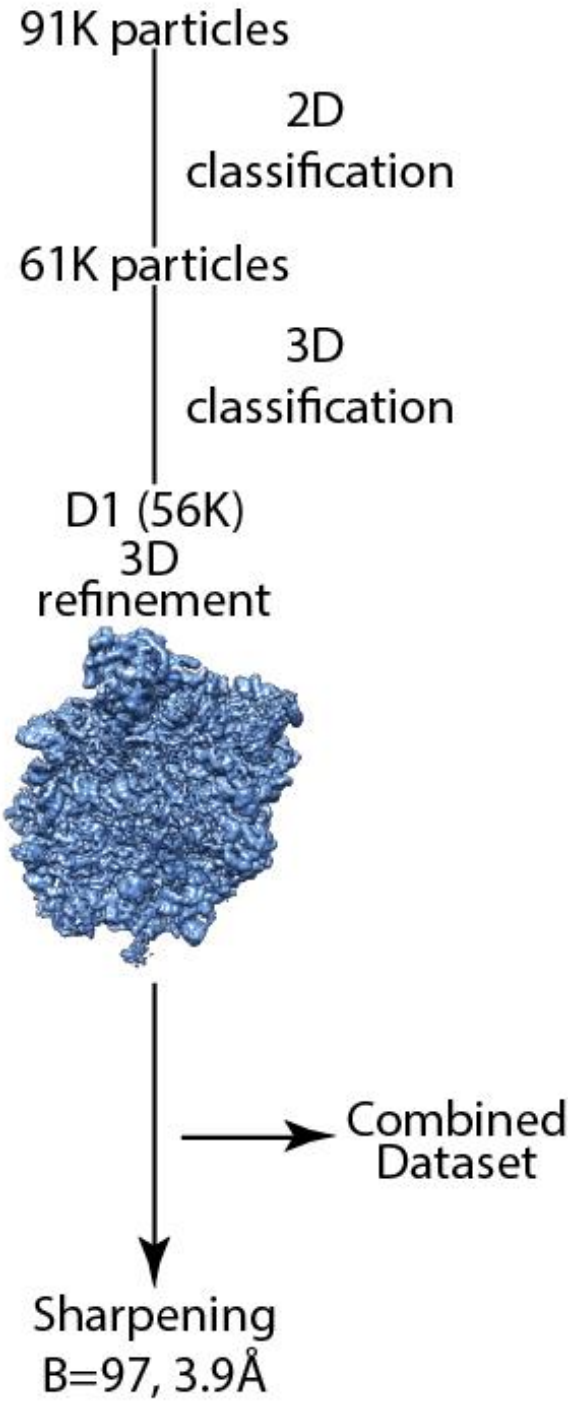

Figure S6. 60S-Nmd3-Lsg1-Tif6 (60SNLT) set 2 processing scheme. No signal subtraction was performed during processing. 56K particles were passed on toward the combined dataset. Refined classes are described in Table S4.

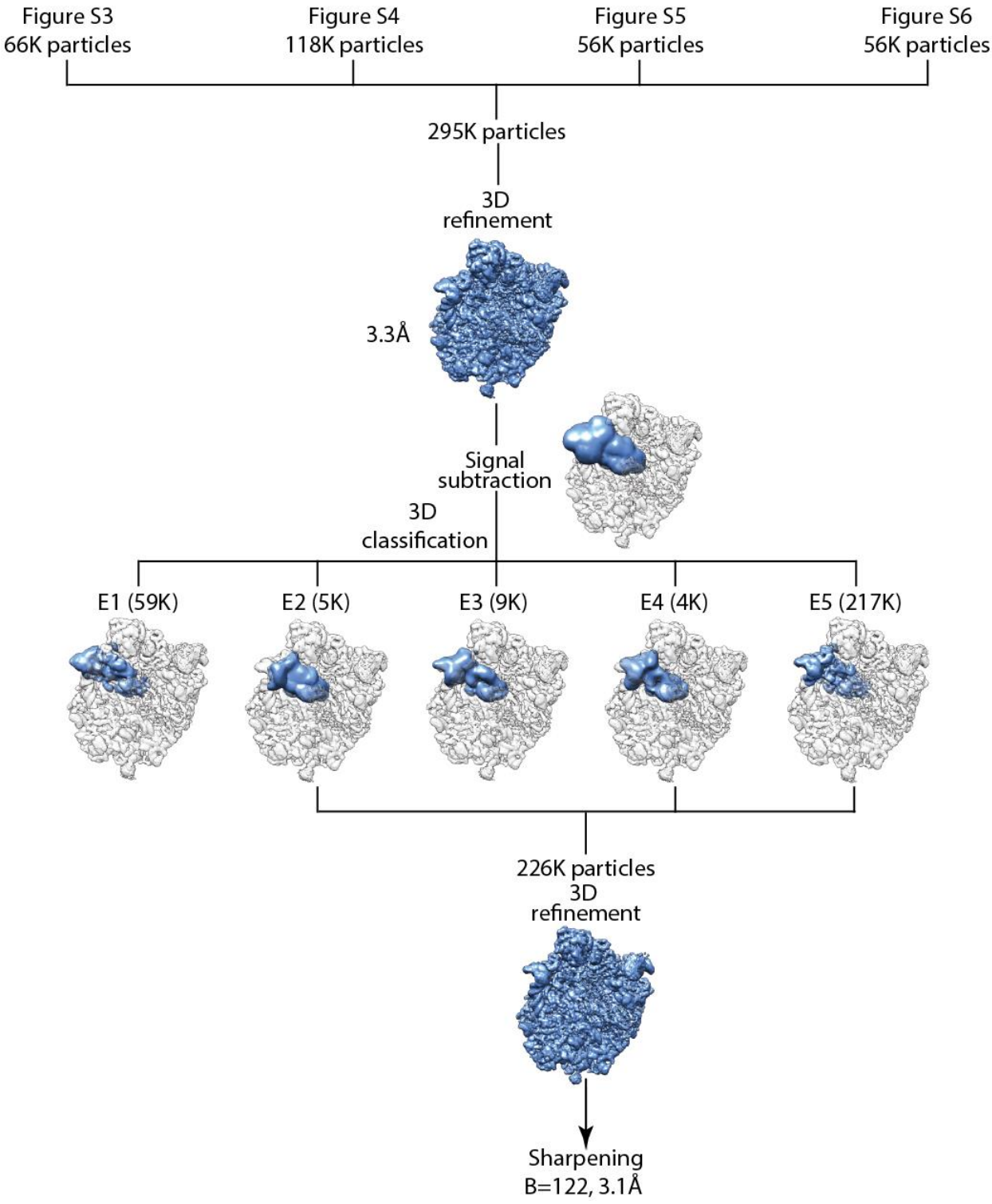

Figure S7. Processing schematic for the combined dataset used to refine a 3.1A map with focus on 60S-Nmd3 density. This map was used as a starting point to build residues 147-401 of Nmd3. The density maintained during signal subtraction is shown in blue.

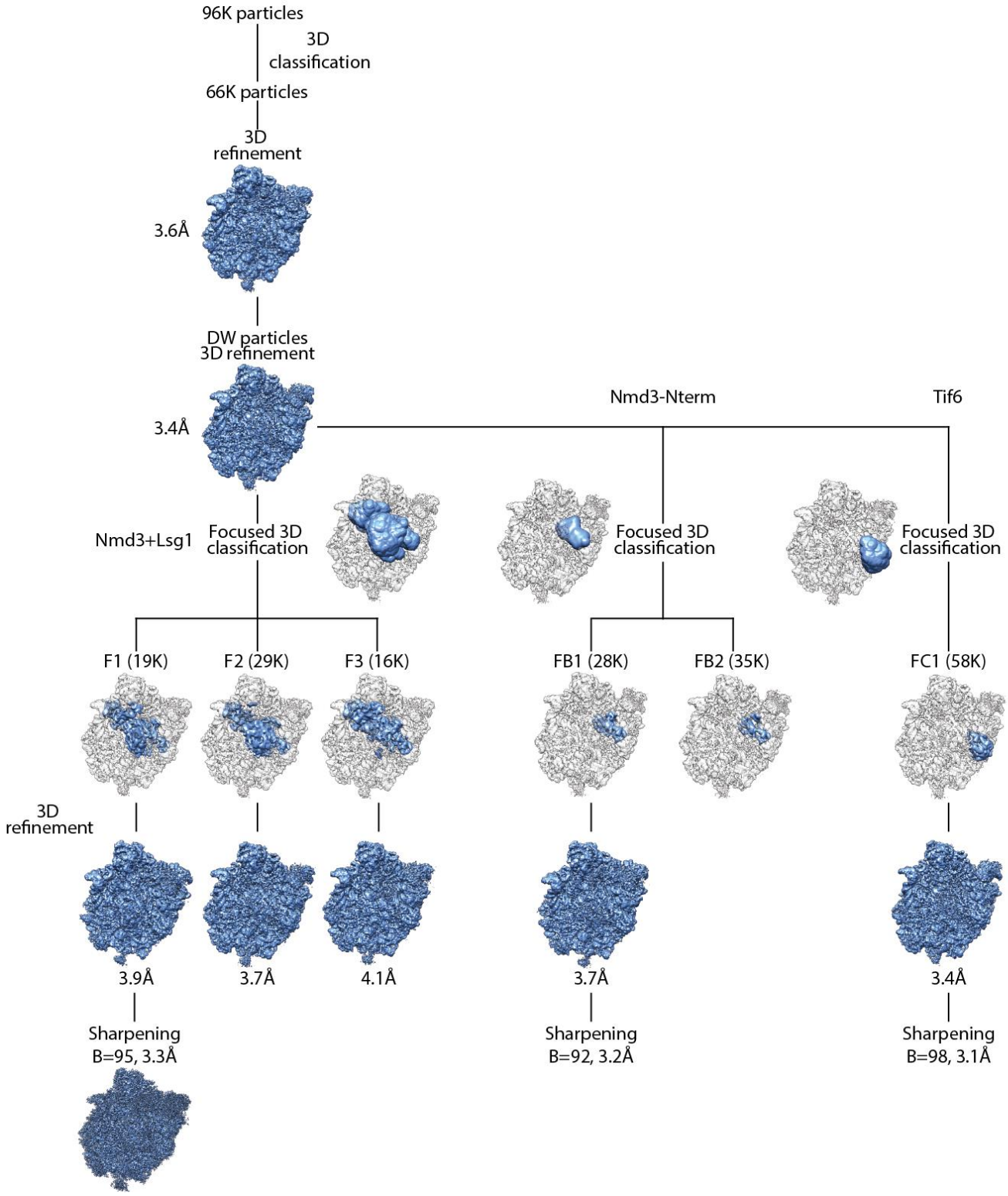

Figure S8. Re-processing scheme for 60S-Nmd3-Lsg1-Tif6 dataset collected on Titan Krios using native pixel size of 1.09 Å/pix, MotionCor2 for frame alignment and Relion2-Beta for processing. The first refinement step was rerun with particles extracted from Dose Weighted micrographs, resulting in initial resolution improvement. Instead of signal subtraction, focused classification was used. The masks used are shown in blue. F1 class was utilized to build Lsg1, and Nmd3 N-terminal domain. Nmd3-Nterm and Tif6 classifications were attempted in order to improve the density of the unbuilt 1-40 residues of Nmd3. While the overall resolution improved, the region of interest did not show significant improvement. Refined classes are described in Table S4.

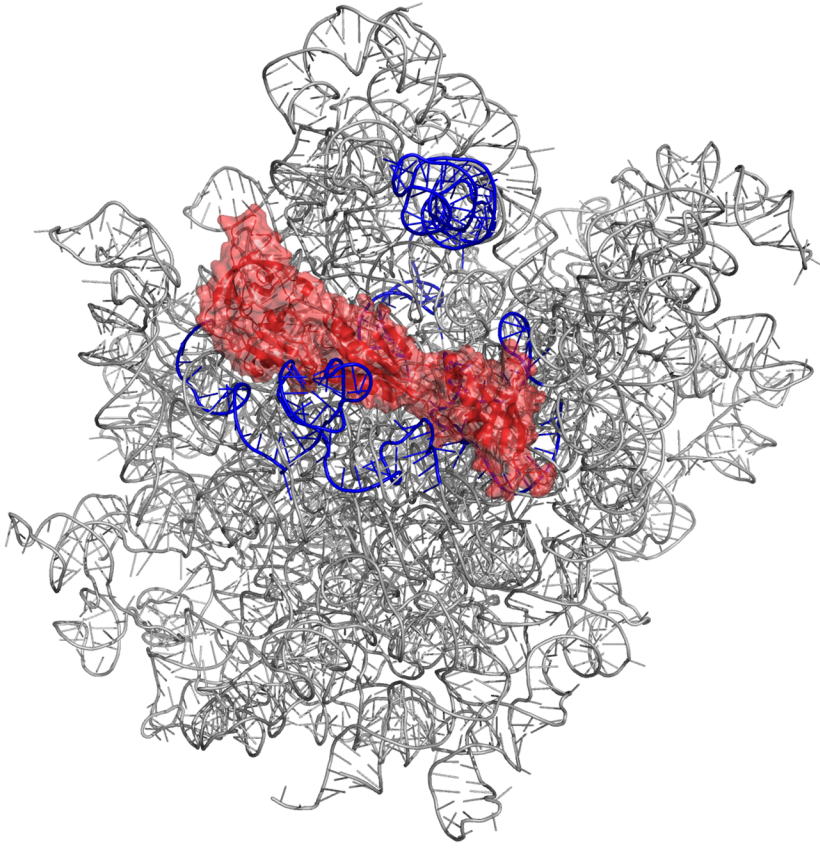

Figure S9. Nmd3 binding site determined by cryo-EM versus UV crosslinking. Nmd3 shown in transparent red and rRNA of the 60S subunit in gray. Reads from UV-induced crosslinking of Nmd3 to rRNA from Matsuo et al (Matsuo et al., 2014) are shown in blue.

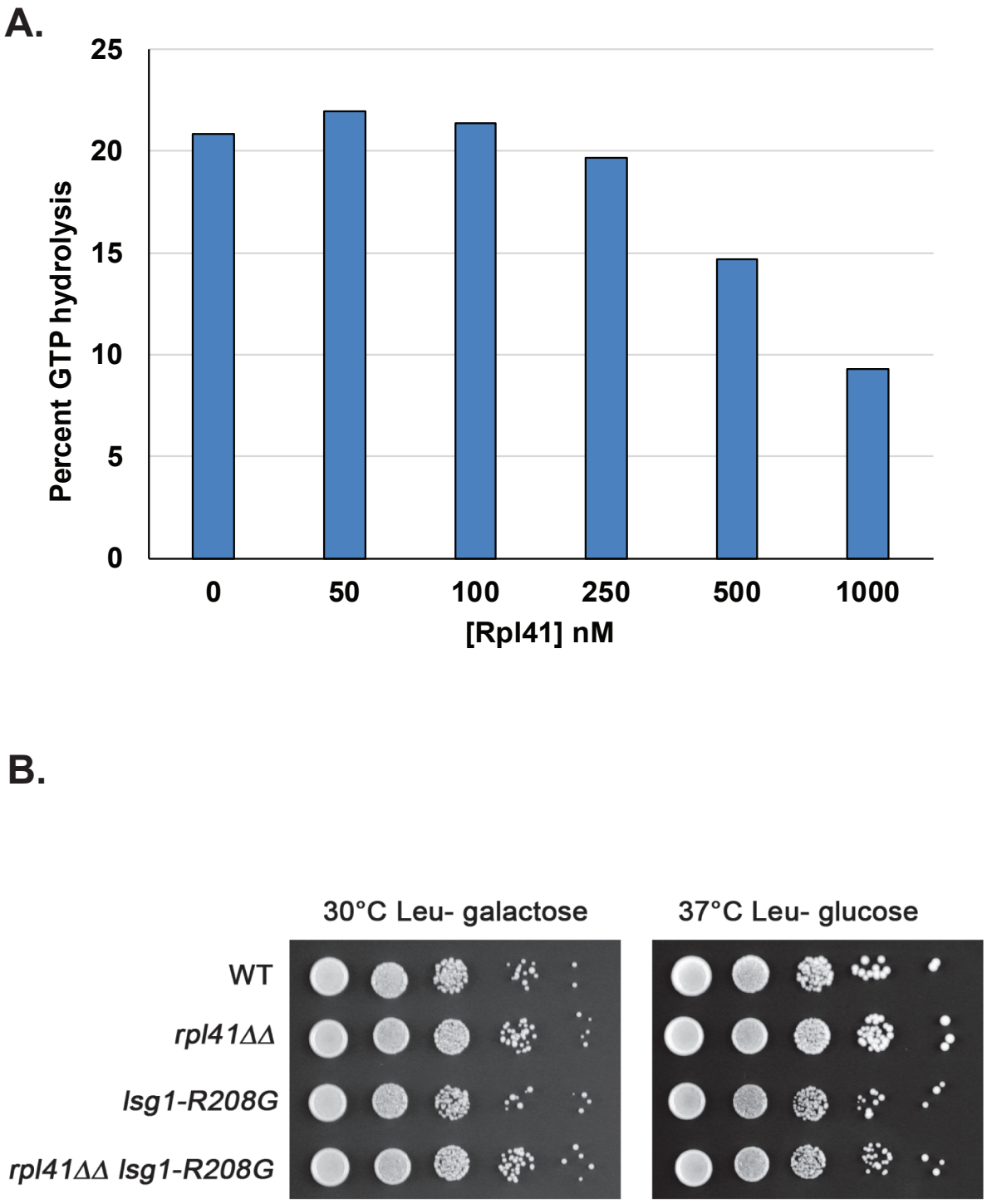

Figure S10. eL41 does not affect Lsg1 function. (A) The GTPase activity of Lsg1 is not stimulated by Rpl41 in vitro. GTPase assays, as described in Methods, contained 50nM 60S, 100nM Nmd3 and 250nM Lsg1. Rpl41 was added to final concentrations ranging from 0.05 to 1uM. Data points are from a single experiment. (B) *LSG1* and *RPL41* do not show genetic interaction. Ten-fold serial dilutions of cultures of WT (AJY3287 (*PGAL-LSG1*) with pAJ2229 expressing WT *LSG1*); *rpl41a*Δ *rpl41b*Δ (*rpl41*ΔΔ) (AJY4073 (*rpl41a*Δ *rpl41b*Δ *PGAL-LSG1*) with pAJ2229); *lsg1-R208G* (AJY328 with pAJ3021 expressing *lsg1-R208G*); and *rpl41a*Δ *rpl41b*Δ *lsg1-R208G* (AJY4073 with pAJ3021). Cells were plated on leucine- plates containing galactose (plating control) or glucose and incubated at 30°C and 37°C, respectively. Cells deleted of *RPL41A* and *RPL41B* showed no apparent growth defect and did not show a synthetic growth defect with *lsg1-R208G*.

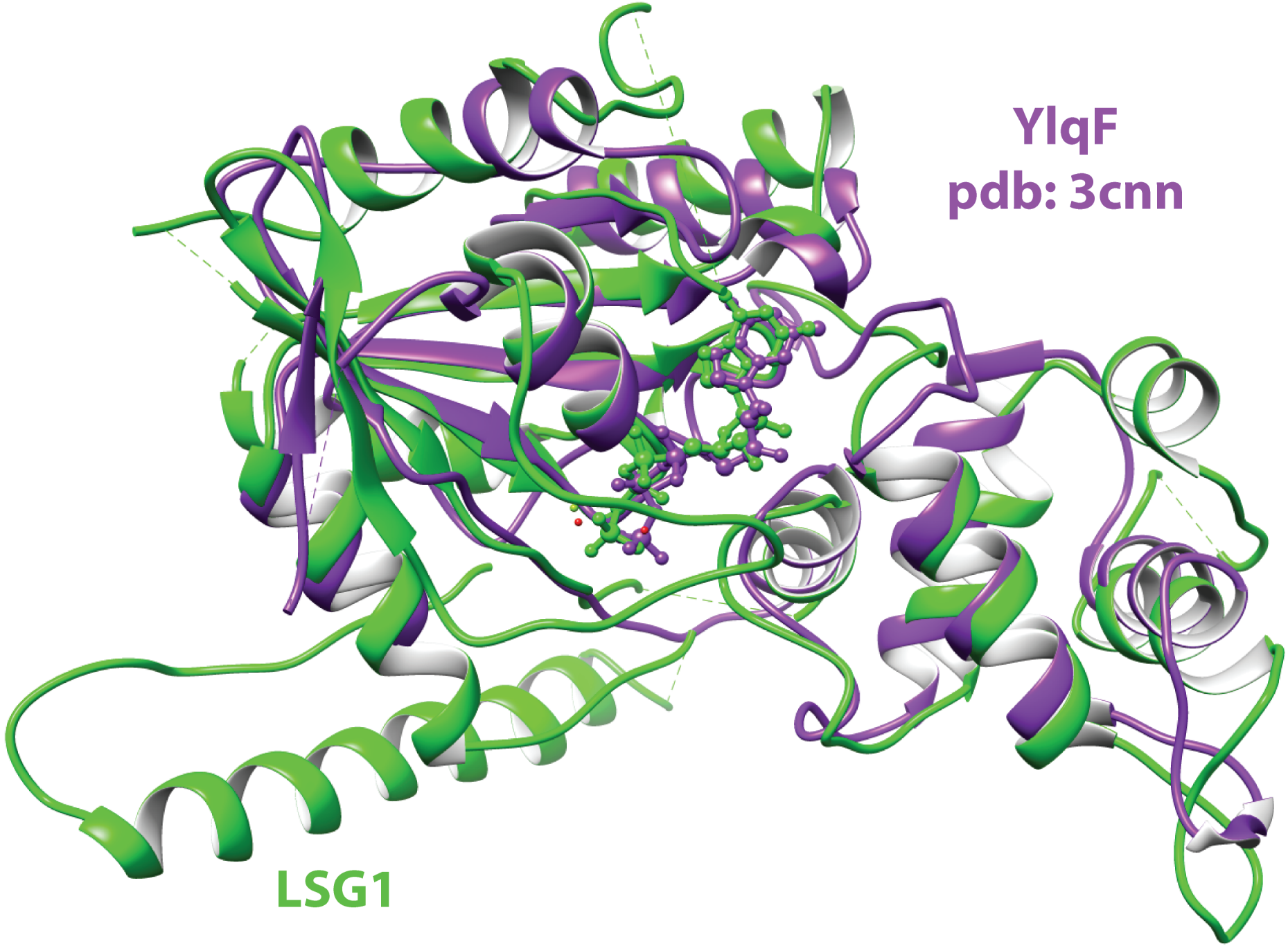

Figure S11. Overlay of Lsg1 and YlqF. Overlay of the Lsg1 model (green) with GTP bound YlqF (pdb:3cnn; purple).

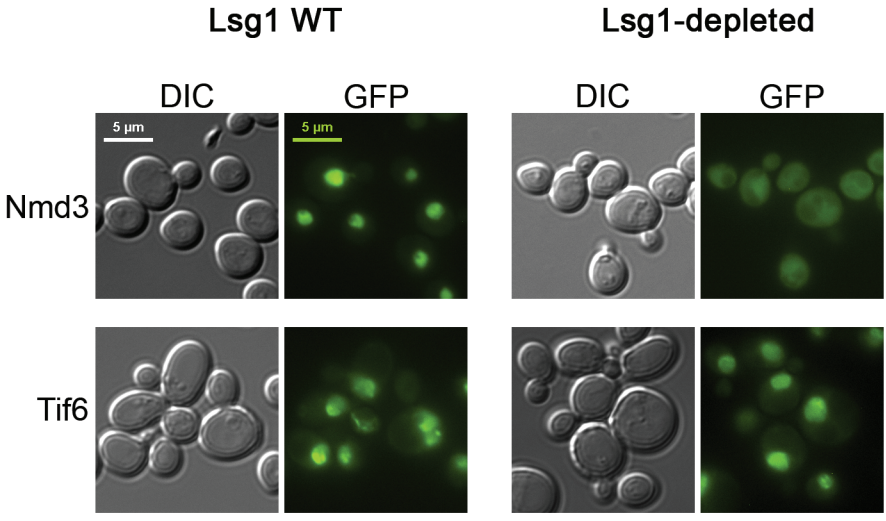

Figure S12. Depletion of Lsg1 traps Nmd3 but not Tif6 in the cytoplasm. The yeast strains AJY3845 (*PGAL1-LSG1 NMD3-GFP CRM1-T539C*) and AJY3842 (*PGAL1-LSG1 TIF6-GFP*) were transformed with plasmids pAJ3760 (WT *LSG1*) or pRS315 (empty vector). Cultures were grown to mid-log phase in synthetic complete medium lacking leucine and containing galactose. Glucose was then added to repress *LSG1* expression and after 6 hr, the localization of Tif6 and Nmd3 was visualized by microscopy. For Nmd3 localization, leptomycin B was added to 0.1 ug/ml final concentration and cells were incubated for an additional 20 min before viewing. Leptomycin B inhibits Crm1-T539C and blocks re-export of Nmd3 if it enters the nucleus. DIC: differential image contrast.

Supplemental Tables

Table S1. Descriptions of various states of L1 stalk, Nmd3, and Lsg1 isolated during processing of the datasets. The default orientation is the one described in the results of the paper: L1 stalk closed, Nmd3 spans from E site towards Tif6. N terminal domain of Nmd3 is in close contact with ribosomal RNA. Lsg1 is centered on Helix 69. (Nmd3 eL22-like and eIF5a-like domains are referred to as domains 2 and 3 respectively).

Sample	Class	Description
60S-Nmd3 Figure S3	A1	L1 stalk fully open, no Nmd3 observed.
	A2	L1 fully closed. Nmd3 domains 2 and 3 are well formed. H38 shows strong density. N-terminal domain and density above domains 2 and 3 only appear at very low threshold levels.
	A3	L1 partially open (T2 state). Nmd3 shows strong density, but poorly resolved. No N-terminal domain.
	A4	L1 almost open (T1 state). Nmd3 domains 2 and 3 region shows some density at low threshold levels.
60S-Nmd3-Lsg1 Figure S4	B1	T2 state. Nmd3 shows strong density, but poorly resolved. No N-terminal domain. Very weak Lsg1.
	B2	T1 state, Nmd3 domains 2 and 3 region shows some density at low threshold levels. No Lsg1 density.
	B3	Default state. Weak Nmd3 N-terminal domain. Low resolution Lsg1 density.
	BB1	Default conformation for L1 stalk and Nmd3 domains 2 and 3. Putative Lsg1 density is disconnected from H69 and located toward and nearly contacting L7/L12 stalk and SRL region. N-terminal domain of Nmd3 is disconnected from 60S and elevated upwards/towards Lsg1 (no elbow region connection visible).

	BB2	Similar to B1, better resolved Lsg1 and Nmd3 N-terminal densities. Well formed H38 and density above domains 2 and 3 of Nmd.

60SNLT Figure S5	C1	T2 state, N-terminal domain of Nmd3 is visible and rolled over towards Lsg1. Well formed H38
	C3	Similar to the default state.

60SNLT set2 Figure S6	D1	Default state with Nmd3 N-terminal domain rolled over towards Lsg1. Elbow is not visible. Well formed H38.
60SNLT reprocess Figure S8	F1	Default orientation of Nmd3 and Lsg1. H38 is strongly deformed and connects to density above Nmd3. uL16 density is missing for residues 3-32, and 93-124.
	F2	Nmd3 N-term is rolled away from 60S towards Lsg1. Lsg1 and H69 are shifted slightly towards the L1 stalk. Well defined H38 density, very limited/noisy density above domains 2 and 3 of Nmd3.
	F3	Partial density for H38, some connection towards density above domain 2 and 3 of Nmd3. Partial density for uL16 (like F1). H69 is pushed toward SRL and down toward H62. Lsg1 is very partial, located in between and above H69 and N-terminal of Nmd3 (moved toward PTC/H38).
	FB1	Default with H38 moving towards Nmd3 and partial density for uL16. Lsg1 is less well resolved compared to F1. Very slight improvement in Nmd3 N terminus.
	FB2	Not refined. The class shows Nmd3 N-terminal rolled towards Lsg1.
	FC3	Default structure. Strong densities for H38, uL16, and density above domains 2 and 3 of Nmd3. Lsg1 is less well resolved, no improvement in Nmd3 N-terminal domain

Table S2. Predicted hydrogen bonds and salt bridges among Nmd3, eL42 and uL1 and comparison with those of eIF5A (PDBePISA server)

			Predicted Hydrogen Bonds (H) / Salt bridges (S)			
Protein 1:2	Interface Residues	Interface Area (Å^2)	#	Prot1	Dist (Å)	Prot2
Nmd3:uL1	22:26	568:586 (577)	H1	TYR 354[OH]	3.58	UNK 154[O]
			H2	ASP 390[O]	3.30	UNK 40[N]
Nmd3:eL42 24:21 751:737 (744)			H1	ASN 380[N]	3.73	THR 64[O]
			H2	ASN 378[ND2]	2.68	CYS 88[O]
			H3	ASN 378[ND2]	3.23	LYS 89[O]
			H4	ASN 378[N]	3.07	LYS 89[O]
			H5	ARG 342[NH1]	3.59	GLU 92[OE1]
			H6	ARG 342[NH1]	3.66	GLU 92[OE2]
			H7	ARG 342[NH2]	3.86	GLU 92[OE2]
			H8	ASN 380[O]	2.58	LYS 61[NZ]
			H9	ASN 378[OD1]	3.31	LYS 66[N]
			H10	SER 377[OG]	3.56	HIS 90[ND1]
			H11	GLN 314[OE1]	2.43	HIS 90[NE2]
			H12	ASN 376[O]	2.68	PHE 91[N]
			H13	ASN 376[OD1]	3.55	PHE 91[N]
			S1	ARG 342[NH1]	3.59	GLU 92[OE1]
			S2	ARG 342[NH1]	3.66	GLU 92[OE2]
			S3	ARG 342[NH2]	3.86	GLU 92[OE2]
			S4	ARG 342[NH1]	3.81	GLU 96[OE2]

eIF5A:uL1	26:31	619:616 (617)	H1	THR 156[OG1]	3.78	UNK 112[O]
eIF5A:eL42	20:21	547:498 (522)	H1	GLU 5 [O]	3.30	LYS 24 [NZ]
			H2	ALA 17[N]	3.57	THR 64[O]

Table S3. Strains used in this study

Strain	Relevant genotype	Source
AJY2188	*MATa rpl41bΔ::KanMX his3Δ1 leu2Δ0 ura3Δ0 met15Δ0*	Research Genetics
AJY2781	*MATa rpl10Δ::KanMX his3Δ1 leu2Δ0 met15Δ0 ura3Δ0*/pAJ2522	This study
AJY3827	*MATalpha Nat-P_{GAL1}-3xHA-LSG1 his3Δ1 leu2Δ0 ura3Δ0*	This study
AJY3842	*MATalpha Nat^r-P_{GAL1}-3xHA-LSG1 TIF6-GFP-His3MX his3Δ1 leu2Δ0 ura3Δ)*	This study
AJY3845	*MAT(not determined) Nat^r-P_{GAL1}-3xHA-LSG1 NMD3-GFP-KanMX CRM1(T539C)-HA*	This study
AJY4066	*MATa rpl41aΔ::Nat his3Δ1 leu2Δ0 ura3Δ0 met15Δ0*	This study
AJY4073	*MATa rpl41aΔ::Nat rpl41bΔ::KanMX His3MX-P_{GAL1}-3xHA-LSG1 his3Δ1 leu2Δ0 ura3Δ0 met15Δ0*	This study
BJ5464	*MATα ura3-52 trp1 leu2Δ1 his3Δ200 pep4::HIS3 prb1Δ1.6R can1*	E. Jones
BY4741	*MATa his3Δ1 leu2Δ0 ura3Δ0 met15Δ0*	Research Genetics

Table S4. Plasmids used in this study

Plasmid	Relevant markers	Source
pAJ1381	P_{GPD}::MBP-TEV-6HIS-*NMD3 LEU2* 2 micron	(Sengupta et al., 2010)
pAJ2229	*LSG1 LEU2 CEN*	This study
pAJ2522	*RPL10 LEU2 CEN*	(Bussiere et al., 2012)
pAJ3021	*lsg1-R208G LEU2 CEN*	This study

pAJ3283	6His-Kemptide-*TIF6*	This study
pAJ3420	*LSG1*-6His	This study
pRS3760	*LSG1 LEU2 CEN*	This study
pRS315	*LEU2 CEN*	(Sikorski & Hieter, 1989)

Table S5. Summary of data collected, particles extracted, number of particles used for classification and refinement

	60S-Nmd3	**60S-Nmd3-Lsg1-Tif6-GMPPNP (60SNLT)**	**60S-Nmd3 Focus Combined Dataset**
Microscope	FEI F-30	FEI Titan Krios	FEI F-30 / Titan Krios
Voltage (kV)	300	300	300
Pixel Size (Å)	1.26	1.1	1.26 / 1.1
Defocus (μm)	1.75-3.75	1-2.5	1-3.75
Particles	65650	19000	226516
Total Images	1296	1443	6301
Used Images	1011	1375	4753
Resolution (Å)	5.8	3.9	3.3
B-factor	119	94	122.2
Resolution after sharpening (Å)	4.3	3.3	3.1

	60SNLT
Clashschore, all atoms	1.6 (100th percentile)
Molprobity Score	2.1 (100th percentile)
Good rotamers (%)	93.7
Ramachandran favored (%)	89
Ramachandran outliers (%)	2.4